Journal of Thermal Science Vol.33, No.1 (2024) 249–267

https://doi.org/10.1007/s11630-023-1875-y **Article ID: 1003-2169(2024)01-0249-19**

Effects of Interaction between Axial and Radial Secondary Air and Reductive Intensity in Reduction Region on Combustion Characteristics and NO_x Emission of Coal Preheated by a Self-Preheating Burner

SU Kun[1,2], DING Hongliang[1,2], OUYANG Ziqu[1,2*], ZHANG Jinyang[1,3], ZHU Shujun[1,2]

1. Institute of Engineering Thermophysics, Chinese Academy of Sciences, Beijing 100190, China
2. University of Chinese Academy of Sciences, Beijing 100049, China
3. School of Energy and Power Engineering, Jiangsu University, Zhenjiang 212013, China

Abstract: The study focused on the effects of the interaction between axial and radial secondary air and the reductive intensity in reduction region on combustion characteristics and NO_x emission in a 30 kW preheating combustion system. The results revealed that the interaction and reductive intensity influenced the combustion in the down-fired combustor (DFC) and NO_x emission greatly. For the temperature distribution, the interaction caused the position of the main combustion region to shift down as $R_{2\text{-}12}$ (ratio of axial secondary air flow to radial secondary air flow) decreased or λ_2 (total secondary air ratio) increased, and there was the interplay between both of their effects. As $R_{3\text{-}12}$ (ratio of first-staged tertiary air flow to second-staged tertiary air flow) increased, the decrease in the reductive intensity also caused the above phenomenon, and the peak temperature increased in this region. For the NO_x emission, the interaction affected the NO_x reduction adversely when λ_2 or $R_{2\text{-}12}$ was higher, and the range of this effect was larger, so that the NO_x emission increased obviously as they increased. The decrease in the reductive intensity caused the NO_x emission increased under the homogeneous reduction mechanism, while was unchanged at a high level under the heterogeneous reduction mechanism. For the combustion efficiency, the interaction improved the combustion efficiency as λ_2 increased when $R_{2\text{-}12}$ was lower, while reduced it as λ_2 increased excessively when $R_{2\text{-}12}$ was higher. The proper decrease in the reductive intensity caused the combustion efficiency increased obviously, while was hardly improved further when the intensity decreased excessively. In this study, the lowest NO_x emission was only 41.75 mg/m^3 without sacrificing the combustion efficiency by optimizing the interaction and reductive intensity.

Keywords: self-preheating; interaction of axial and radial secondary air; reductive intensity; combustion characteristic; NO_x emission

1. Introduction

In China, coal is the main energy [1], and its main utilization of the coal is thermal power generation, which is an effective guarantee for human life and industrial development [2]. Nevertheless, most of pollutants, especially NO_x, are produced during combustion of carbon-based fuels, which affects many aspects adversely

Received: May 21, 2022 AE: YANG Bin Corresponding author: OUYANG Ziqu E-mail: ouyangziqu@iet.cn

in the life [3, 4]. On the one hand, excessive NO_x emission is the main cause of acid rain, leading to the soil acidification and loss of soil mineral nutrients, so that food production is endangered [5]. On the other hand, NO_x can cause human respiratory diseases due to the irritating odor and toxicity. Hence, exploring the methods to reduce the NO_x emission has been an urgent problem for every country to solve.

At present, coal-fired denitrification technologies are mainly divided into two types: in-combustion and post-combustion denitrification technologies. Among them, the former mainly contain low-temperature combustion, staged combustion, low-NO_x burner, exhaust gas recycle and flameless combustion technologies [6–15]. Though these traditional technologies can reduce the NO_x emission, the effect is relatively limited. The latter mainly contain selective catalytic reduction (SCR) and selective non-catalytic reduction (SNCR) technologies, whose denitrification efficiency is more than 70% [16–18]. Nevertheless, the applicability and economics are relatively poor due to some disadvantages, such as narrow operating temperature window, high cost and secondary pollution [19]. By contrast, the in-combustion denitrification technologies have greater development potential in these aspects, which promotes the construction of ecological civilization greatly. Hence, attaching importance to the research on the in-combustion denitrification technologies is more beneficial to the development of economy and industry.

Air-staged combustion technology, as one of the in-combustion denitrification technologies, has been utilized widely. The basic principle is that the combustion of pulverized coal is occurred in the primary reduction region, and the NO_x generation is inhibited effectively in this region due to the lower temperature and O_2 concentration [20, 21]. Moreover, the coal gas generated in this region is also conducive to the subsequent NO_x reduction. Afterwards, the residual fuel is entered into the burnout zone, and mixed with the over fire air to burn out. Researchers have launched some research on this technology, and found that it has good applicability and denitration capability [8, 22, 23]. Hence, it was necessary to explore this technology in depth.

The Institute of Engineering Thermophysics, Chinese Academy of Science has proposed the self-preheating combustion technology, which borrows partly from the principle of the air-staged combustion technology. With this technology, the multistage combustion air is introduced into a self-preheating burner and a DFC, which are the main equipment in the self-preheating system, to realize the multistage combustion of pulverized coal and multistage directional reduction of coal-N. Researchers have launched plenty of research on this technology on bench-scale and pilot-scale test rigs, and the results reveal that it can realize the clean and efficient combustion of pulverized coal [24–31].

According to the air-staged combustion technology, the reduction region, as the key region for the removal and directional reduction of coal-N, influenced the efficient and clean combustion significantly [20, 21]. Hence, the distribution of the secondary and tertiary air, as the main factor affecting the reduction region, had been investigated a lot [24, 25, 28]. Moreover, on this basis, the effects of reactant and combustion air jet velocities on the self-preheating combustion characteristics and NO_x emission were also explored further under the depth air classification, and found adjusting them properly could improve the denitrification capacity in the reduction region and optimize the follow-up combustion of the residual coal char [32]. Nevertheless, in the previous studies, the effects of the interaction between multistage combustion air in the DFC were often ignored under this air distribution. Among them, the interaction between the axial and radial secondary air affected the position of core region and potential flow region of the combustion air at the top of the DFC, and thus affected the combustion of the preheated fuel and the removal and thermal conversion of coal-N in this region [33]. The interaction between the first-stage and second-stage tertiary air, as the key factor affecting the reductive intensity in the reduction region, also influenced the removal of coal-N in this region [20, 23]. Hence, it was necessary to explore the effects of the interaction between the multistage combustion air in depth. In terms of the deficiencies of previous research, this study focused on the influences of the interaction between axial and radial secondary air and the reductive intensity in the reduction region on combustion characteristics and NO_x emission by varying λ_2, $R_{2\text{-}12}$ and $R_{3\text{-}12}$ on a 30 kW self-preheating combustion test rig with the objective to promote the removal and directional reduction of coal-N fully in the reduction region, and thus realize the ultra-low NO_x emission (lower than 50 mg/m^3) during combustion. Experimental results were the improvement and supplement to the previous research, and provided guidance for the optimization of NO_x control strategy in coal-fired power plants.

2. Experimental Section

2.1 Experimental apparatus

The experimental system, the schematic diagram of which was consistent with that in Ref. [32], was composed of a self-preheating burner and a DFC.

The self-preheating burner was designed with the archetype of a circulating fluidized bed, whose advantages contained fuel flexibility, good reactive stability and low cost, and its outside was wrapped by

insulation cotton to reduce heat loss [34]. The pulverized coal was fed into the riser which was 90 mm in inner diameter and 1500 mm in height by a screw feeder, and then it was mixed with primary air. Its temperature was generally heated to 800°C–950°C only by the heat released from combustion and gasification reactions [25, 27, 35]. In this process, the pulverized coal was modified into coal char and coal gas (collectively called preheated fuel).

The preheated fuel generated during preheating was entered into the DFC which was 300 mm in inner diameter and 3500 mm in height to burn out. To reduce the NO_x emission further during the subsequent combustion, combined with air-staged technology, two types of the secondary air nozzles and two layers of the tertiary air nozzles were utilized in the DFC. Among them, the secondary air nozzles were an axial secondary air nozzle (located at the top of the DFC) and a radial secondary air nozzle (located at 500 mm), respectively (their specific schematic diagrams were referred to Ref. [32]). The axial secondary air nozzle adopted the design of multi-channel coaxial jet nozzle with a 1:1 relationship between the inner and external secondary air, and the radial secondary air nozzle adopted the design of ring-shaped hedging nozzle. Two tertiary air nozzles were the first-staged tertiary air nozzle (located at 1000 mm) and the second-staged tertiary air nozzle (located at 1500 mm), both of which had the same structure as the radial secondary air nozzle.

5 K-type and 10 S-type thermocouples, the position distribution of which had been listed in Ref. [32], were utilized to acquire the real-time temperature change in the self-preheating burner and DFC. The measurement range for the former was 0–1100°C, and that for the latter was 0–1600°C. The position of sampling apertures had been introduced in previous researches [25, 26]. Among them, the preheated fuel was collected from the sampling aperture at the outlet of the self-preheating burner and utilized for analyzing the preheating properties. The compositions in the preheated coal gas were analyzed by Agilent 3000A Micro GC. The flue gas, composed of CO, CO_2, NO, NO_2 and O_2, was sampled at the sampling apertures along the DFC. For measuring the flue gas compositions, O_2 was measured with a KM 9106 analyzer and other compositions were measured with a Fourier infrared gas analyzer. The instrumental error was within ±2%. The fly ash was collected from the water cooler and utilized for the calculation of the combustion efficiency. In this study, each case had stable operation for about 1.5 h, and the temperature fluctuation of each measurement was within ±5°C during sampling.

2.2 Fuel characteristics

In the study, Shenmu bituminous coal was selected as the experimental raw material, and its properties are listed in Table 1. Additionally, Fig. 1 shows the particle size distribution of the raw coal.

Table 1 Proximate and ultimate analysis of Shenmu bituminous coal

	Ultimate analysis /% (air dry) (weight percent)				
Items	C	H	O	N	S
Date	72.44	4.06	11.13	1.02	0.55
	Proximate analysis /% (air dry) (weight percent)				
Items	M	A	V	FC	
Date	5.06	5.74	32.37	56.83	

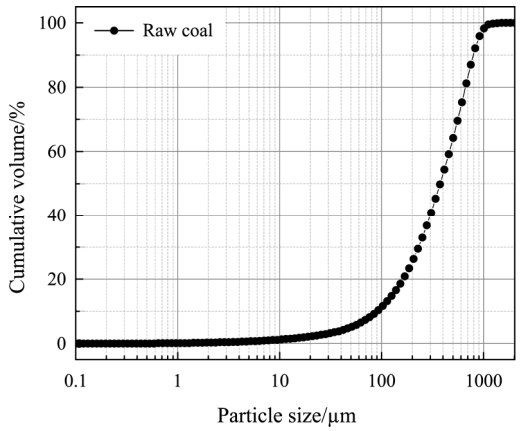

Fig. 1 Particle size distribution of Shenmu bituminous coal

2.3 Experimental conditions

Table 2 and Table 3 list all the cases. In these tables, λ_P, λ_2, λ_3 and λ are denoted as the ratios of primary air, secondary air, tertiary air and total air, respectively. λ_P, the thermal load and the fuel feed rate are fixed at 0.35, 42.84 kW and 5.50 kg/h, respectively.

The experimental variables included λ_2, $R_{2\text{-}12}$, and $R_{3\text{-}12}$. Among them, the influence of the interaction of axial and radial secondary air was investigated by varying λ_2 and $R_{2\text{-}12}$ (as listed in Table 2). The interaction was regulated by varying the total secondary air flow for the former, while by varying the two-stage secondary air distribution for the latter, which could analyze the influence of the interaction systematically from multiple perspectives. Moreover, it was worth noting that increasing $R_{2\text{-}12}$ not only resulted in the redistribution of the two-stage secondary air flow, but also changed the two-stage secondary air jet velocities, which were the key factors affecting flow field and combustion at the top of the DFC [32, 36]. Mei found that the primary and secondary air jet velocities affected the flame temperature distribution and NO_x emission under the moderate or intense low oxygen dilution combustion of pulverized coal [37]. Liu found that the primary and tertiary air jet velocities influenced

the NO_x distribution along the boiler by the combination of numerical simulation and experiments on a 1000 MW double-tangential-circle boiler [38]. Thong focused on the effects of ratio of jet to cross momentum ratio on mixing and turbulence intensity, and found that this ratio affected the core and potential flow regions greatly [33]. The results indicated that the change in the two-stage secondary air jet velocities affected gas-solid reactant flow, combustion and pollutant emission greatly, so that it was necessary to investigate the effect of the interaction by varying $R_{2\text{-}12}$ on the subsequent combustion with the self-preheating combustion technology. The influence of the reductive intensity in the reduction region was investigated by varying $R_{3\text{-}12}$ (as listed in Table 3), and as $R_{3\text{-}12}$ increased, the intensity decreased gradually due to the introduction of first-staged tertiary air. According to the research on different variables, all the cases were divided into 9 groups to analyze the experimental results better (as listed in Table 4).

Table 2 Experimental conditions of effect of the interaction of axial and radial secondary air

Items	M_1	λ_p	M_{21}	M_{22}	$R_{2\text{-}12}$	λ_2	M_3	$R_{3\text{-}12}$	λ_3	M	λ
Unit	m^3/h	–	m^3/h	m^3/h	–	–	m^3/h	–	–	m^3/h	–
Case 1	13.80		0.00	15.77	0.00		17.75			47.32	
Case 2	13.79		3.94	11.83	0.33		17.74			47.30	
Case 3	13.81	0.35	7.89	7.89	1.00	0.40	17.75	0.00	0.45	47.34	1.20
Case 4	13.82		11.83	3.94	3.00		17.74			47.33	
Case 5	13.80		15.77	0.00	∞		17.75			47.32	
Case 6	13.80		0.00	19.71	0.00		13.80			47.31	
Case 7	13.80		4.93	14.78	0.33		13.80			47.31	
Case 8	13.79	0.35	9.86	9.86	1.00	0.50	13.81	0.00	0.35	47.32	1.20
Case 9	13.78		14.78	4.93	3.00		13.79			47.28	
Case 10	13.81		19.71	0.00	∞		13.80			47.32	
Case 11	13.80		0.00	23.66	0.00		9.86			47.32	
Case 12	13.80		5.91	17.75	0.33		9.85			47.31	
Case 13	13.80	0.35	11.83	11.83	1.00	0.60	9.85	0.00	0.25	47.31	1.20
Case 14	13.81		17.75	5.91	3.00		9.86			47.33	
Case 15	13.82		23.66	0.00	∞		9.85			47.33	

Note: M_1: Primary air flow (m^3/h); M_{21}: Axial secondary air flow (m^3/h); M_{22}: Radial secondary air flow (m^3/h); M_3: Tertiary air flow (m^3/h); M: Total air flow (m^3/h); $R_{2\text{-}12}$: The ratio of M_{21} to M_{22}

Table 3 Experimental conditions of the effect of reductive intensity in the reduction region

Items	M_1	λ_p	M_{21}	M_{22}	$R_{2\text{-}12}$	λ_2	M_{31}	M_{32}	$R_{3\text{-}12}$	λ_3	M_3
Unit	m^3/h	–	m^3/h	m^3/h	–	–	m^3/h	m^3/h	–	–	m^3/h
Case 1	13.80			15.77			0.00	17.75	0.00		17.75
Case 16	13.79			15.76			4.44	13.31	0.33		17.75
Case 17	13.80	0.35	0.00	15.77	0.00	0.40	8.88	8.88	1.00	0.45	17.76
Case 18	13.81			15.78			13.31	4.44	3.00		17.75
Case 19	13.80			15.77			17.75	0.00	∞		17.75

Note: M_{31}: First-staged tertiary air flow (m^3/h); M_{32}: Second-staged tertiary air flow (m^3/h); $R_{3\text{-}12}$: The ratio of M_{31} to M_{32}

Table 4 Experimental groups

Experimental groups	1	2	3	4	5	6	7	8	9
Experimental condition	Case 1	Case 2	Case 3	Case 4	Case 5	Case 1	Case 6	Case 11	Case 1
						Case 2	Case 7	Case 12	Case 16
	Case 6	Case 7	Case 8	Case 9	Case 10	Case 3	Case 8	Case 13	Case 17
	Case 11	Case 12	Case 13	Case 14	Case 15	Case 4	Case 9	Case 14	Case 18
						Case 5	Case 10	Case 15	Case 19

3. Results and Discussions

3.1 Operation stability of the self-preheating burner

The temperature variation in the self-preheating burner is shown in Fig. 2. The temperature fluctuation of each temperature measurement point was within ±5°C, and the maximum temperature difference at different locations was less than 50°C. The maximum measured temperature (called the preheating temperature) was 892°C.

Fig. 3 shows the differential pressure fluctuations at different positions in the self-preheating burner. Among them, P_{12} was denoted as the differential pressure from 100 mm to 500 mm; P_{23} was denoted as the differential pressure from 500 mm to 1450 mm, and P_{34} was denoted as the differential pressure between the inlet and the outlet of the cyclone separator. The green line was the filtering curve, which could reflect the stability of pressure in the burner. Hence, combined with the preheating temperature variation, the small temperature fluctuation and the smooth filtering curves of the differential pressure indicated the self-preheating burner could operate stably for a long time. Additionally, the relationship of differential pressure at different locations was: $P_{34}>P_{12}>P_{23}$, which was related to the particle concentration distribution directly. With the stable operation of the self-preheating burner, sparse phase and dense phase regions were formed in the upper and lower parts of the riser respectively, and P_{12} was lower due to the lower particle concentration in the sparse phase. Compared to P_{12} and P_{23}, P_{34} always remained a high level due to the higher inlet velocity of cyclone separator [39].

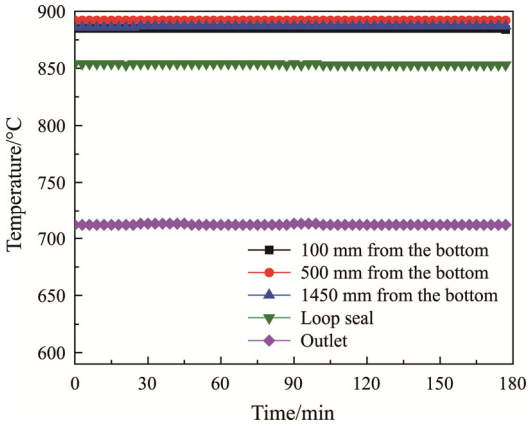

Fig. 2 Temperature variation in the self-preheating burner

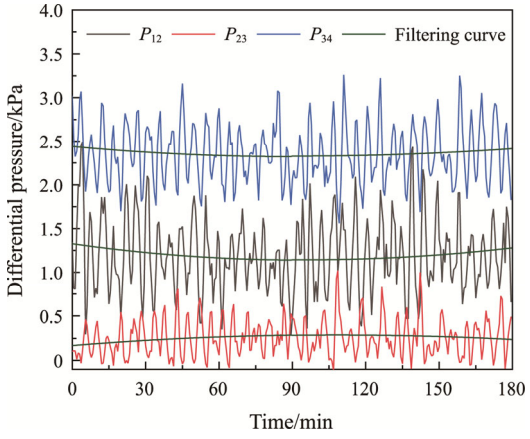

Fig. 3 Differential pressure fluctuation in the self-preheating burner

The small temperature fluctuation and the smooth filtering curves of the differential pressure indicated the self-preheating burner could operate stably for a long time. Furthermore, the temperature at the outlet of the burner was high enough, which ensured the rapid ignition and efficient combustion of the preheated fuel in the DFC.

Table 5 lists the compositions in the preheated coal gas at the outlet. It could be found that they mainly contained N_2, CO_2, CH_4, H_2 and CO. Among them, the content of N_2 was the highest, 68.47%, while the content of CH_4 was the least, only 1.25%. NO_x (NO and NO_2) and O_2 were not detected, indicating this process was in a strongly reducing atmosphere. Hence, most of the released fuel-N was converted into N_2, and a small part was converted into HCN and NH_3. Additionally, the content of NH_3 was 513.34 mg/m^3, while the content of HCN was only 30.01 mg/m^3, indicating NH_3 was the main form of NO_x precursor. The reason might be that the conversion of fuel-N to NH_3 was promoted at about 890°C [35]. Moreover, HCN was hydrogenated by H_2O in the pulverized coal and converted into NH_3 by R1 [40].

$$HCN + H_2O \rightarrow NH_3 + CO \qquad (R1)$$

The combustible gases in the coal gas incorporated CO, H_2, and CH_4, with average volume fractions of

Table 5 Composition analysis of high temperature coal gas (dry base)

Coal gas main compositions	Content
CO/% (vol)	10.30
CO_2/% (vol)	13.60
H_2/% (vol)	6.38
CH_4/% (vol)	1.25
N_2/% (vol)	68.47
O_2/% (vol)	0.00
NO/mg·m^{-3}	0.00
NO_2/mg·m^{-3}	0.00
N_2O/mg·m^{-3}	0.00
NH_3/mg·m^{-3}	513.34
HCN/mg·m^{-3}	30.01
Q_L/MJ·m^{-3}	2.59

10.30%, 6.38%, and 1.25%, respectively. Its calorific value was 2.59 MJ/m^3, and the higher calorific value could accelerate the ignition of preheated fuel.

3.2 The effect of interaction of axial and radial secondary air on combustion characteristics and NO_x emission

In this study, the axial and radial secondary air were introduced at the top and 500 mm in the DFC, respectively. Base on their nozzle structure, the former could increase the radial contact area between the preheated fuel and combustion air and promote their slow mixing and combustion, and the latter could enhance the mixing intensity of reactants in the vicinity of 500 mm [27, 41, 42]. Moreover, both of the jet directions were vertical mutually, which contributed to the formation of a cross jet in the reduction region, and thus stabilized and intensified the combustion of the preheated fuel and accelerated the release and thermal conversion of coal-N in this region [43]. Hence, owing to the respective advantages and synergy of the two-stage secondary air, in-depth exploration of the interaction between the axial and radial secondary air was very necessary.

λ_2 and $R_{2\text{-}12}$ were the key factors affecting this interaction. By varying λ_2 and $R_{2\text{-}12}$, the respective actions and the position of the cross jet core region of the two-stage secondary air were influenced greatly, and thus the combustion characteristics and release of coal-N were also influenced. The effects of the interaction regulated by λ_2 and $R_{2\text{-}12}$ were discussed and analyzed in detail in the follow.

3.2.1 The effect of interaction regulated by λ_2

3.2.1.1 Temperature distribution

Fig. 4 shows the effect of the interaction regulated by varying λ_2 on the temperature distribution along the DFC. All temperature curves showed the trend of increasing first and then decreasing. When $R_{2\text{-}12}$>1.00, the peak temperature points were located at 600 mm. When $R_{2\text{-}12}$= 0.33 and 1.00, they were located at 600 mm under λ_2 = 0.40 and 0.50, while at 800 mm under λ_2 = 0.60. When $R_{2\text{-}12}$=0.00, as λ_2 increased from 0.40 to 0.60, they were shifted down gradually and located at 600 mm, 800 mm and 1200 mm, respectively. The results indicated that when $R_{2\text{-}12}$ was lower, the main combustion region was shifted down gradually as λ_2 increased, while the phenomenon wasn't obvious when $R_{2\text{-}12}$ was higher, which was mainly because the two-staged secondary air distribution could affect the regulation of λ_2 on the interaction to some extent. When $R_{2\text{-}12}$ was higher, the axial secondary air was dominant. Based on its nozzle structure, the combustion air was diffused into a large radial space and the combustion of reactants was relatively slow, so that the combustion was relatively mild, which weakened the influence of λ_2 on the upper combustion [25]. Hence, increasing λ_2 had less effect on the position of the main combustion region. When $R_{2\text{-}12}$ was lower, the radial secondary air was dominant, and its action space was concentrated in the vicinity of 500 mm. Hence, a great deal cold air was introduced in this region as λ_2 increased in this condition, which decreased the temperature of reactants, and thus slowed down the combustion of preheated fuel and shifted the main combustion region down. Additionally, the temperature gradually decreased above 600 mm as λ_2 increased. On the one hand, it was also due to the absorption of heat by the cold air. On the other hand, too high combustion air flow could affect radiative heat transfer adversely, and thus reduce the combustion reaction rate [44]. Below 1600 mm, the temperature increased gradually as λ_2 increased, which was mainly caused by the difference in combustion share entered into this region. In the study, since λ_p was fixed at 0.35, the original combustion share entered into the DFC was basically the same under different cases. Hence, the temperature decreased in the upper part of the DFC as λ_2 increased, meaning the combustion share decreased in this region, and corresponding more heat was released in the lower part of the DFC.

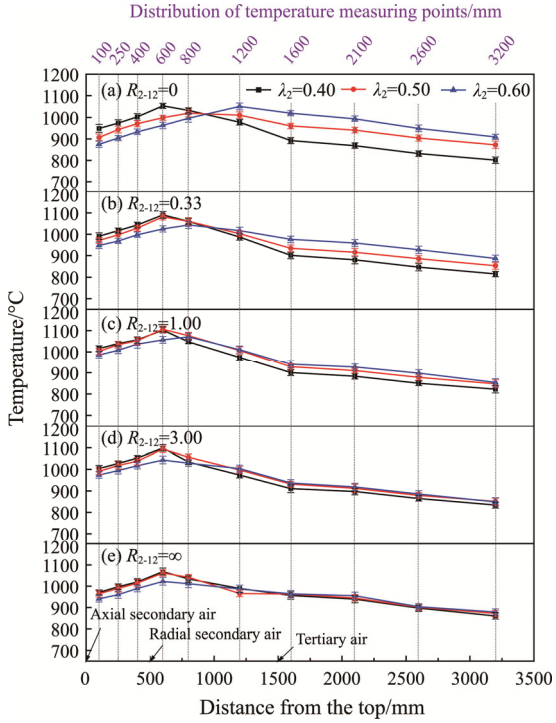

Fig. 4 The temperature distribution along the DFC

3.2.1.2 Flus gas analysis

Fig. 5 shows the effect of the interaction regulated by varying λ_2 on the concentrations of O_2, CO_2 and CO along the DFC. Evenly distributed with a peak value less

than 7% above 1400 mm, the low O_2 concentrations could inhibit NO_x generation effectively. Above 900 mm, when $R_{2\text{-}12}\leq 1.00$, O_2 concentrations remained at an extremely low level first and then increased, while they increased first, then decreased, and then increased again when $R_{2\text{-}12}>1.00$, meaning that the two-stage secondary air distribution influenced the combustion intensity greatly in this region. When $R_{2\text{-}12}$ was lower, less O_2 supplied from the top of the DFC was consumed rapidly by the coal gas, while when $R_{2\text{-}12}$ was higher, the mixing and combustion of reactants was slow in the upper part of the DFC based on this secondary air distribution, which reduced the O_2 consumption rate, and then this rate was accelerated with the adequate mixing of reactants. In the region of 900–2400 mm, with the introduction of the tertiary air at 1500 mm, O_2 concentration increased gradually under different $R_{2\text{-}12}$. Below 2400 mm, O_2 concentration still showed a trend of decreasing, meaning that the combustion region continued to be amplified, which contributed to the more uniform temperature distribution [27].

At 150 mm, CO_2 was generated in large quantities with the rapid ignition and combustion of the high-temperature preheated fuel (especially CO), so that CO_2 concentration was much higher than the original concentration in the coal gas. The extremely low O_2 concentration in this position also indicated the intense combustion was occurred. Afterwards, CO_2 concentration begun to decrease in the upper part of the DFC due to the dilution of the flue gas and the reduction of the combustion intensity. In the region of 900–2400 mm, CO_2 concentration decreased except $R_{2\text{-}12}=\infty$ due to the dilution of the flue gas by the tertiary air, while increased slightly when $R_{2\text{-}12}=\infty$. When $R_{2\text{-}12}=\infty$, the content of combustible components in residual char entered into this region was relatively high as the combustion was slow and mild in the upper part of the DFC, leading that the more organic carbon was converted into CO_2 in this region. Below 2400 mm, all the CO_2 concentrations decreased again. Additionally, when $R_{2\text{-}12}$ was fixed, the change of CO_2 concentration curves was very little under different λ_2, indicating that the interaction regulated by varying λ_2 had less effect on the CO_2 concentration distribution.

The trends of CO concentration curves under different λ_2 were basically the same. Above 900 mm, owing to the rapid homogeneous consumption of CO, its concentration decreased rapidly to a low level. Afterwards, the concentration almost remained constant. Hence, it could be inferred the coal gas was almost exhausted before the introduction of the tertiary air, and NO_x was mainly reduced by the coal char in the lower part of the DFC.

Fig. 6 shows the effect of the interaction regulated by varying λ_2 on NO_2 and NO concentrations along the DFC. NO_2 concentrations showed basically the same trend: decreasing to a low level first, and then almost remaining constant. NO_2 was unstable, easily decomposed at high temperature, and it was mainly generated in the fuel-rich zone [45]. Hence, owing to the inadequate mixing of reactants at 150 mm, the local fuel-rich region was formed, so that NO_2 was generated in large quantities. Afterwards, the generated NO_2 was consumed and decomposed continuously at high temperature. The main NO_2 generation and consumption reactions are shown in R2–R4 [46]. Furthermore, the difference of NO_2 concentration curves was unconspicuous under different λ_2, indicating that the interaction regulated by varying λ_2 had less effect on the distribution of NO_2 concentration.

$$NO + HO_2 \rightarrow NO_2 + OH \quad (R2)$$

$$O + NO_2 \rightarrow NO + O_2 \quad (R3)$$

$$H + NO_2 \rightarrow NO + OH \quad (R4)$$

Compared to NO_2, the variation pattern of NO concentration was more complicated. At 150 mm, NO concentration was significantly lower than NO_2 concentration. The reason was that there was a competitive relationship between the generation of NO and NO_2, and fuel-N tended to be converted into NO_2 in the oxygen-poor atmosphere of this position [45], so that correspondingly the NO generation was inhibited. In the region of 0–400 mm, λ_2 had different effects on the NO concentration distribution under different $R_{2\text{-}12}$. When $R_{2\text{-}12}\leq 1.00$, NO concentration decreased, and λ_2 had less effect on it. When $R_{2\text{-}12}=3.00$, the change of NO concentration under different λ_2 was obvious in this region. Among them, when $\lambda_2=0.40$, NO concentration decreased, while it increased obviously when $\lambda_2=0.50$ and 0.60. When $R_{2\text{-}12}=\infty$, NO concentration under different λ_2 showed a trend of increasing in this region, and it increased as λ_2 increased at 400 mm. The results indicated that the interaction regulated by increasing λ_2 could weaken the reductive atmosphere in this region, leading that the NO concentration in the flue gas increased, and this effect was more obvious when $R_{2\text{-}12}$ was higher. Afterwards, in the region of 400–2400 mm, the change of NO concentration was relatively complicated under different λ_2, which was due to the synergy of the complicated thermochemical conversion of fuel-N and the generation and reduction of NO. Nevertheless, it was worth noting that when $R_{2\text{-}12}$ was higher, NO concentration remained a high level consistently in this region with the increase of λ_2. Hence, it could be inferred that the adverse influence of the interaction regulated by increasing λ_2 on the NO reduction wasn't limited to the region at the top of the DFC, while was extended to the bottom of the DFC all the way. Below 2400 mm, NO concentration decreased gradually under the heterogeneous reduction by the coal char.

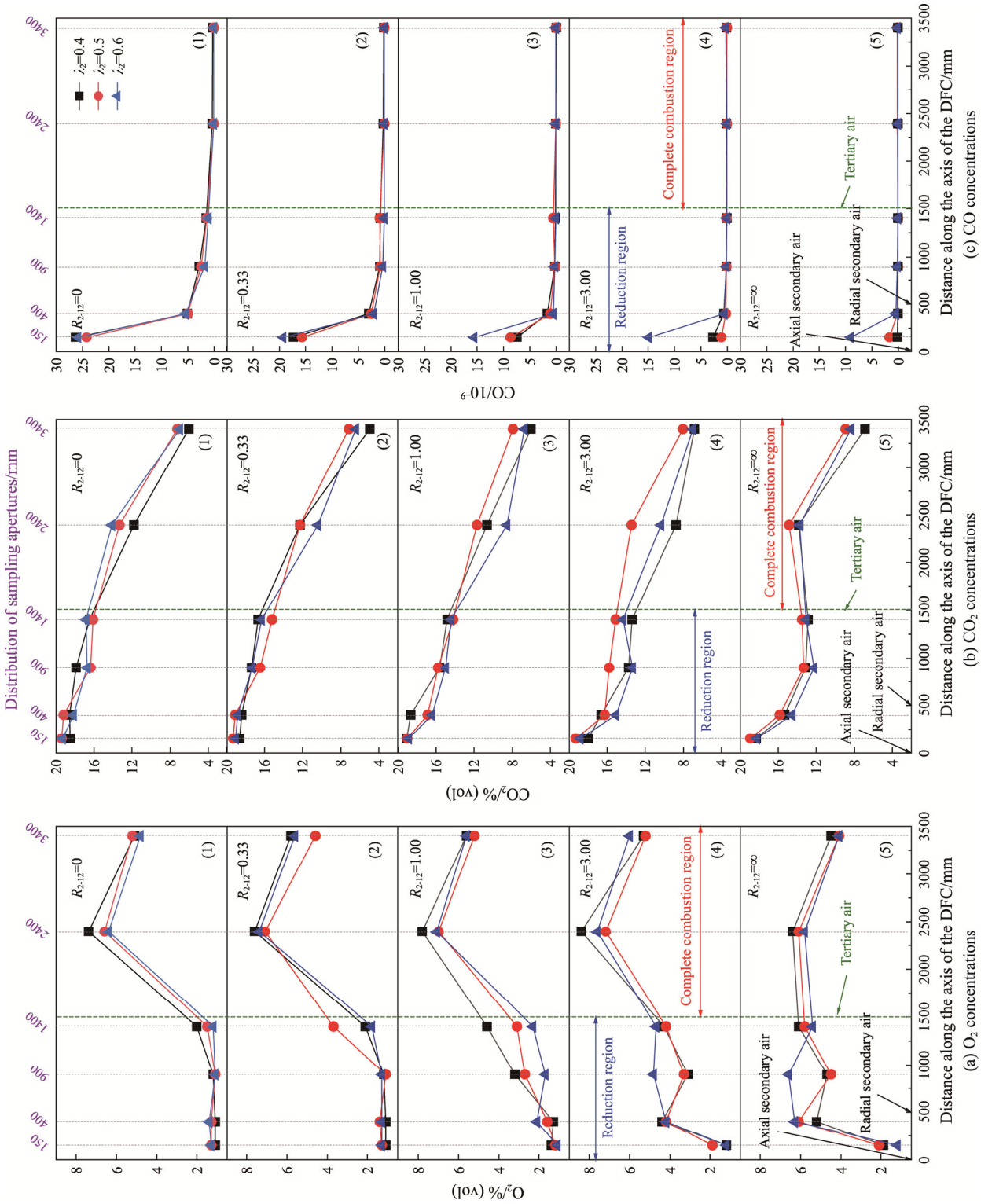

Fig. 5 O_2, CO_2 and CO concentrations along the DFC

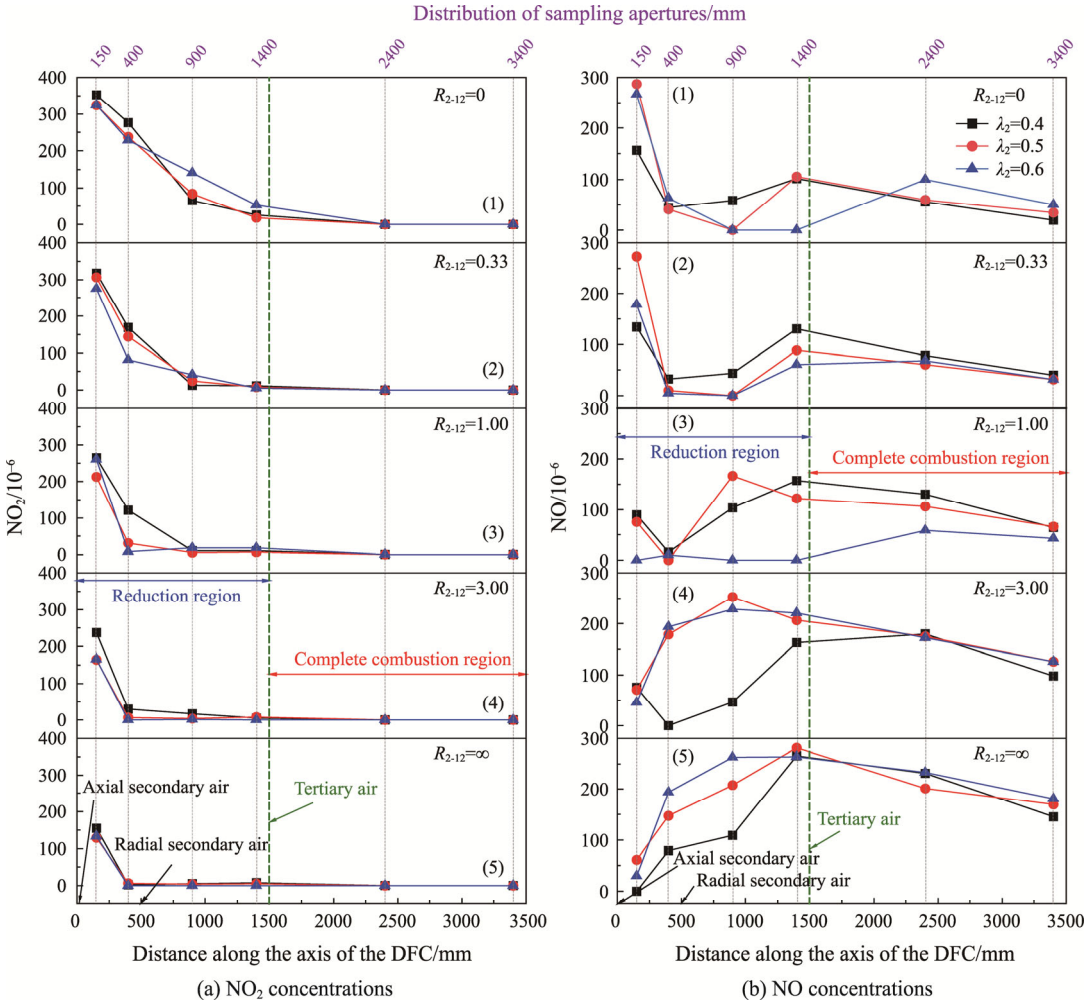

Fig. 6 NO_2 and NO concentrations along the DFC

3.2.1.3 Combustion efficiency and NO_x emission

Fig. 7 shows the effect of the interaction regulated by varying λ_2 on combustion efficiency and NO_x emission. As λ_2 increased, the NO_x emission variation pattern under different $R_{2\text{-}12}$ was different, indicating that the two-stage secondary air distribution influenced the effect of this interaction on the thermal conversion of coal-N along the DFC and the subsequent NO_x emission. When $R_{2\text{-}12}\geq 3.00$, NO_x emission increased as λ_2 increased and always stayed at a high level, while it always remained a low level when $R_{2\text{-}12}<3.00$. The reason was mainly that when $R_{2\text{-}12}$ was higher, the secondary air distribution influenced the NO_x reduction adversely in the larger region of the DFC, and this effect was reinforced gradually as λ_2 increased, so that NO_x reduction efficiency decreased in the DFC. Nevertheless, when $R_{2\text{-}12}$ was lower, a large amount of coal-N had been released and converted into NO_x at the top of the DFC, which prolonged the NO_x reduction time [24]. Additionally, when $R_{2\text{-}12}$ was lower, the NO_x emission had different change trends as λ_2 increased. Among them, the NO_x emission decreased under $R_{2\text{-}12}$=0.33 and 1.00, while increased under $R_{2\text{-}12}$=0, meaning that the axial secondary air supply was necessary for the NO_x reduction emission. For the former, a small amount of axial secondary air promoted the release of coal-N above 500 mm at the high temperature, and increasing λ_2 could intensify this action. Meanwhile, the inadequate axial secondary air had less impact on the residence time and CO consumption, so that increasing λ_2 could promote the release and reduction of coal-N in this condition. For the latter, the secondary air was only introduced from the radial secondary air nozzle. Under this air distribution, the local oxygen-rich region might be formed in the vicinity of 500 mm. Increasing λ_2 could not only intensify this action, but also weaken the reductive intensity of the reduction region, which limited the action of the reduction region greatly.

Combustion efficiency was defined as the ratio of heat released by the incomplete combustion to heat released by complete combustion [47]. The specific formulas were as follows:

$$\eta = 100 - q_3 - q_4 \tag{1}$$

$$q_3 = \frac{C_f}{100 - C_f} \times \frac{33\ 727 A_{ar}}{Q_{net,ar}} \times 100\% \quad (2)$$

$$q_4 = \frac{V_{gy} \times 123.36CO}{Q_{net,ar}} \times 100\% \quad (3)$$

where η was combustion efficiency, %; q_3 was the heat loss of solid incomplete combustion, %; q_4 was the heat loss of gas incomplete combustion, %; V_{gy} was the flow of the exit flue gas, m^3/kg; C_f was the combustible percentage of fly ash.

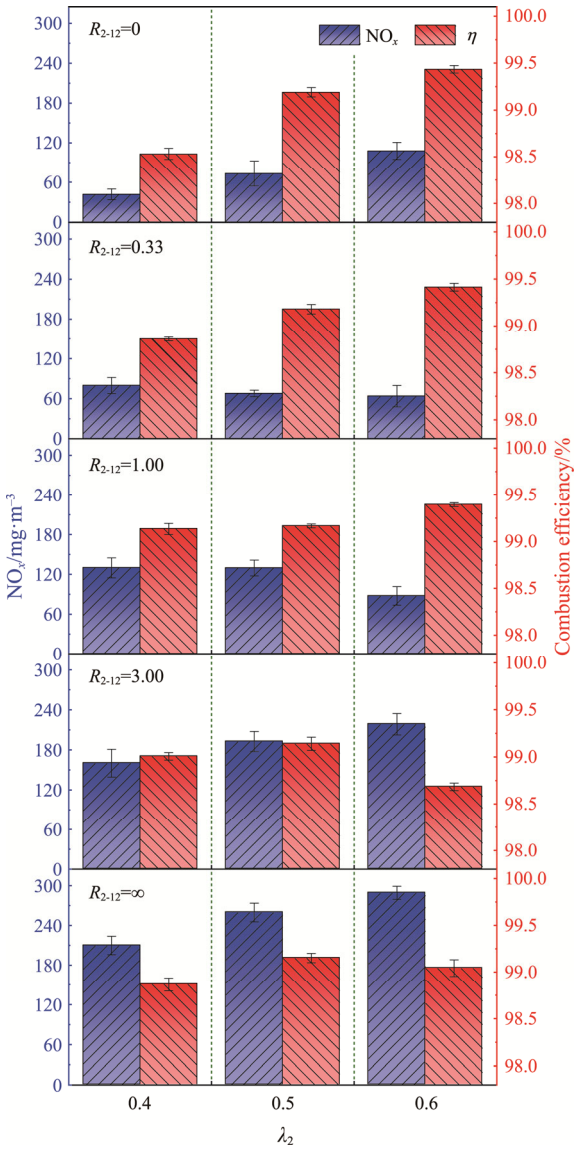

Fig. 7 Combustion efficiency and NO_x emission

Under different $R_{2\text{-}12}$, the combustion efficiency had different change regularity as λ_2 increased, meaning the effect of the interaction on the combustion efficiency was also affected by the secondary air distribution. When $R_{2\text{-}12} \leq 1$, the combustion efficiency increased as λ_2 increased, while it increased first and then decreased, and reached the maximum under λ_2=0.50 when $R_{2\text{-}12}$>1. When $R_{2\text{-}12}$ was lower, more combustion air was introduced from the radial secondary air nozzle as λ_2 increased, which prolonged the mixing and combustion time of reactants greatly under this air distribution. Nevertheless, when $R_{2\text{-}12}$ was higher, this two-stage secondary air distribution influenced the mixing and combustion of reactants adversely in the upper part of the DFC, and this effect was regulated greatly by λ_2. Among them, when λ_2 was lower, the adverse effect wasn't obvious due to the introduction of a small amount of the secondary air, so that increasing λ_2 properly could still prolong the combustion time, and thus improve the combustion efficiency. Nevertheless, when λ_2 was higher, the adverse effect was reinforced severely. Increasing λ_2 could shorten the residence time of the preheated fuel obviously, and thus the combustion was deteriorated continuously.

In conclusion, the interaction regulated by varying λ_2 affected the combustion efficiency and NO_x emission greatly, and this effect was regulated by the two-staged secondary air distribution to some extent. When $R_{2\text{-}12}$ was lower, increasing λ_2 properly could improve combustion efficiency while the NO_x emission remained a low level. Nevertheless, when $R_{2\text{-}12}$ was higher, increasing λ_2 excessively might cause the combustion efficiency and NO_x emission decreased and increased respectively, so that the combustion of the preheated fuel was deteriorated severely.

3.2.2 The effect of interaction regulated by $R_{2\text{-}12}$

3.2.2.1 Temperature distribution

Fig. 8 shows the effect of the interaction regulated by varying $R_{2\text{-}12}$ on the temperature distribution along the DFC. When $R_{2\text{-}12}$=0.00 and ∞, namely the secondary air was introduced only from a single nozzle, the temperature above 600 mm was lower, while it increased significantly under other $R_{2\text{-}12}$, which demonstrated that the staged secondary air could adjust the position of the core region of the secondary air and optimize the interaction, and thus the upper combustion was improved. The following was a comparative analysis on the temperature distribution in the region of 0–800 mm when $R_{2\text{-}12}$=0.00 and ∞. Among them, the temperature for the former was significantly less than that for the latter. The reason was that as the secondary air wasn't introduced timely for the former, the mixing and combustion of the preheated fuel was delayed, which reduced the combustion share in this region. Hence, the earlier introduction of the secondary air was very necessary for the upper combustion. Additionally, the interaction could influence the position of the main combustion region greatly; this effect was also regulated by λ_2. Under

different $R_{2\text{-}12}$, the peak temperature points were always located at 600 mm when λ_2=0.40. When λ_2=0.50, the peak point was shifted down to 800 mm under $R_{2\text{-}12}$= 0.00, while the points were still located at 600 mm under other $R_{2\text{-}12}$. When λ_2=0.60, the peak points were still located at 600 mm under $R_{2\text{-}12}\geq$3.00, while the points were shifted down to 800 mm and 1200 mm when 0.00< $R_{2\text{-}12}$<3.00 and $R_{2\text{-}12}$=0.00, respectively. The results indicated that decreasing $R_{2\text{-}12}$ could shift the position of the main combustion region down, and this influence was reinforced by increasing λ_2. As $R_{2\text{-}12}$ decreased, the radial secondary air was gradually dominant. In this condition, the inadequate O_2 supplement above 500 mm slowed down the combustion. Additionally, a large amount of cold air was introduced intensively in the vicinity of 500 mm, so that the ignition and combustion of the preheated fuel were delayed obviously in this region, and increasing λ_2 could intensify this action further.

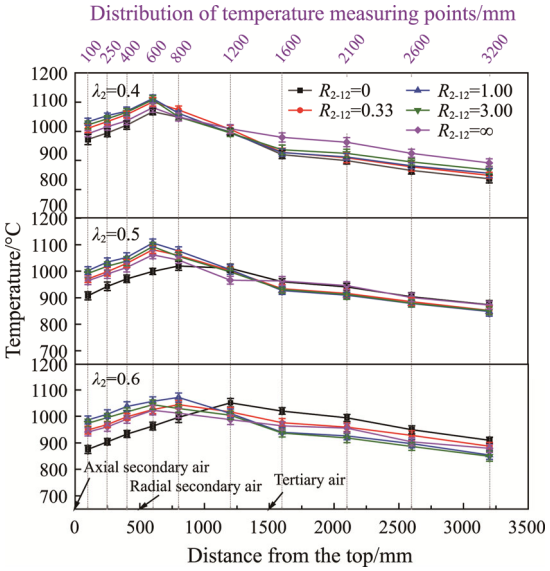

Fig. 8 The temperature distribution of the DFC

3.2.2.2 Flus gas analysis

Fig. 9 shows the effect of the interaction regulated by varying $R_{2\text{-}12}$ on the concentrations of O_2, CO_2 and CO along the DFC. In the region of 0–900 mm, O_2 concentration increased gradually as $R_{2\text{-}12}$ increased when $R_{2\text{-}12}\geq$1.00, while it always remained a low level when $R_{2\text{-}12}$<1.00, indicating that the two-stage secondary air influenced the O_2 concentration distribution greatly in this region. When $R_{2\text{-}12}$ was higher, the mixing and combustion of reactants was slowed due to too high proportion of the axial secondary air flow as $R_{2\text{-}12}$ increased, leading that the O_2 consumption rate decreased. Nevertheless, when $R_{2\text{-}12}$ was lower, since the axial secondary air flow was lower, O_2 was consumed rapidly by coal gas above 500 mm, and then with the introduction of a large amount of the radial secondary air, the mixing of reactants could be intensified obviously in the vicinity of 500 mm based on this nozzle structure, so that O_2 in the combustion air was consumed rapidly again. With the introduction of the tertiary air at 1500 mm, O_2 concentration increased slightly in this region when $R_{2\text{-}12}$=∞ in the region of 1400–2400 mm, while increased significantly under other $R_{2\text{-}12}$, which might been mainly due to the difference of the combustion intensity. Below 2400 mm, O_2 concentration decreased due to the combustion of the residual char.

Above 400 mm, CO_2 concentration decreased obviously along the DFC when $R_{2\text{-}12}\geq$1.00, while it only decreased slightly when $R_{2\text{-}12}$<1.00, which was mainly due to the different levels of the high-temperature coal gas consumption in this region. As shown in Fig. 9(c), the decrease of CO concentration when $R_{2\text{-}12}\geq$1.00 was much smaller than that when $R_{2\text{-}12}$<1.00 in this region, indicating that the amount of the coal gas involved in the CO_2 generation was lower for the former, so that the CO_2 content in the flue gas decreased. In the region of 900–1400 mm, the change of CO_2 concentration was slight. The reason might be that the reduction region was formed with the gradual mixing of reactants, and CO_2 concentration was mainly regulated by the synergy of the combustion reaction of C with O_2 and the gasification reaction of C with CO_2 [48]. Afterwards, with the introduction of the tertiary air, CO_2 concentration decreased significantly due to the dilution of the flue gas in the region of 1400–2400 mm, while it increased slightly when $R_{2\text{-}12}$=∞. The two-stage secondary air distribution for the latter caused the mixing, and combustion of reactants was slow in the upper part of the DFC, so that the content of combustible components in the residual char entered into the lower part was higher and more organic carbon was converted into CO_2 by the combustion, which counteracted the dilution of the flue gas partially.

CO concentration decreased rapidly to a low level first, and then almost remained constant. As $R_{2\text{-}12}$ increased, the position where CO concentration decreased to a low level was shifted upwards gradually, meaning CO was depleted earlier, and this phenomenon was more obvious when λ_2 was higher. The reason was mainly that with more axial secondary air introduced from the top of the DFC accelerated the early homogeneous consumption of the coal gas as $R_{2\text{-}12}$ increased; moreover, increasing λ_2 could increase the axial secondary air flow further, and thus reinforce this effect.

Fig. 10 shows the effect of the interaction regulated by varying $R_{2\text{-}12}$ on NO_2 and NO concentrations along the DFC. At 150 mm, NO_2 concentration decreased gradually as $R_{2\text{-}12}$ increased. NO_2 was mainly generated in the fuel-rich atmosphere, which was weakened gradually in

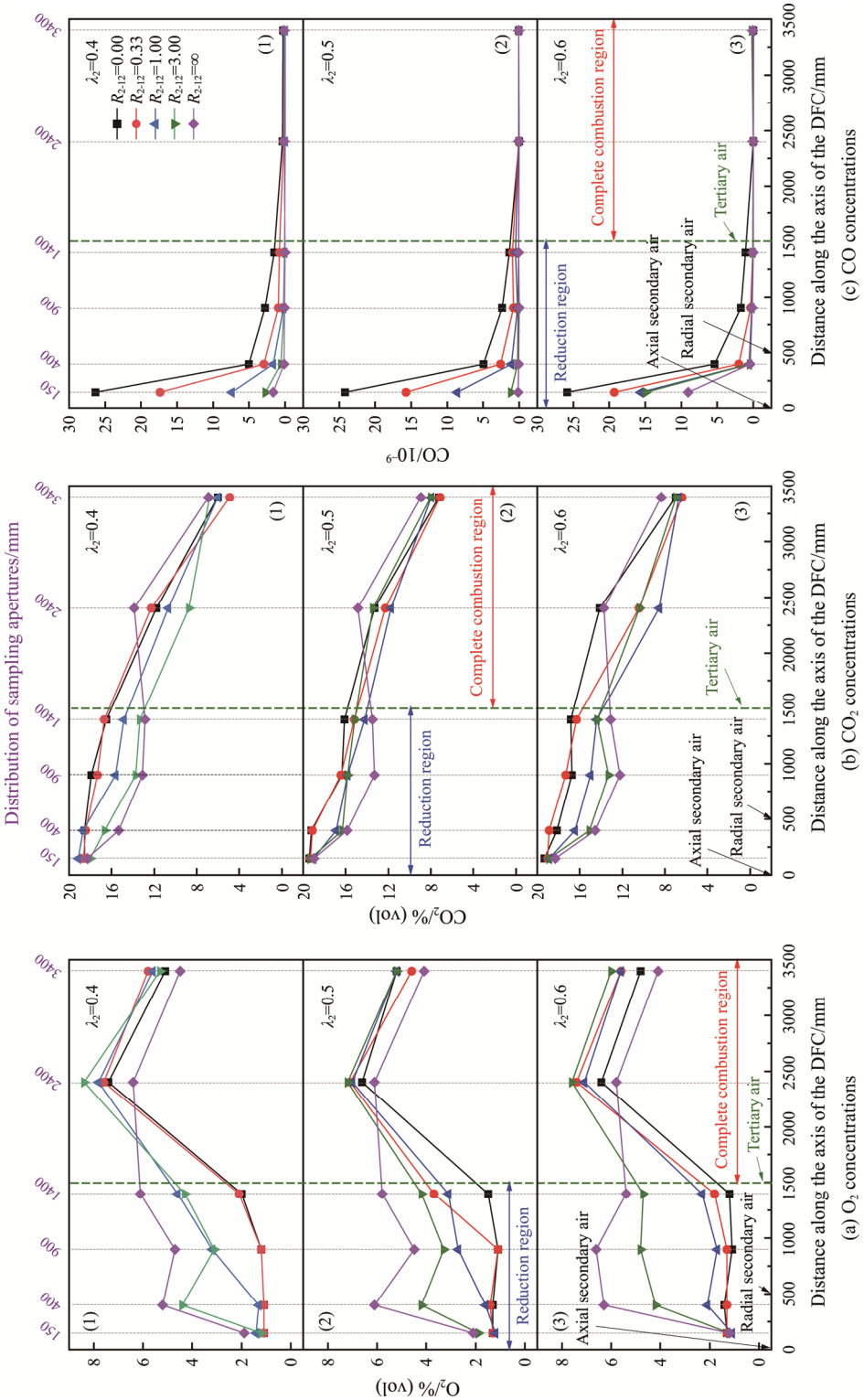

Fig. 9 O_2, CO_2 and CO concentrations along the DFC

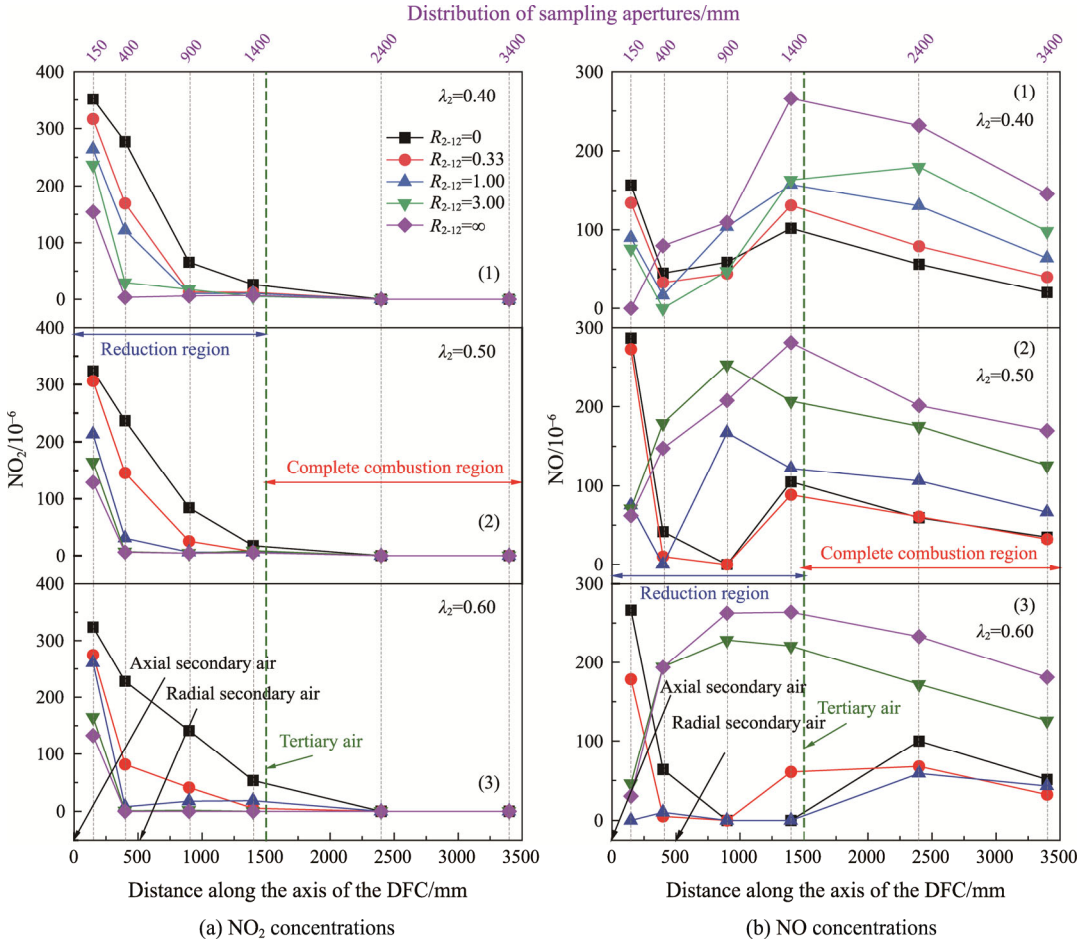

Fig. 10 NO_2 and NO concentrations along the DFC

this position due to the increase in the proportion of the axial secondary air as $R_{2\text{-}12}$ increased, so that NO_2 generation was inhibited [49]. In addition, as $R_{2\text{-}12}$ increased, the position where NO_2 concentration decreased to a low level was shifted upwards. Hence, the results demonstrated that increasing $R_{2\text{-}12}$ was detrimental to the conversion of coal-N to NO_2 in the upper part of the DFC.

The change trend of NO concentration was relatively complex under different $R_{2\text{-}12}$. At 150 mm, NO concentration was much higher under $R_{2\text{-}12}$<1.00 than that under other $R_{2\text{-}12}$, and NO_2 concentration was also higher for the former, meaning that lower $R_{2\text{-}12}$ might promote the early release and conversion of fuel-N. In the region of 150–900 mm, NO concentration decreased rapidly first, and then remained constant or decreased slightly when $R_{2\text{-}12}$<1.00, while it increased when $R_{2\text{-}12}$=∞, which was mainly due to the difference of the reduction intensity in this region. As shown in Fig. 9(c), CO concentration was relatively high above 400 mm when $R_{2\text{-}12}$<1.00, indicating that there was a strong reductive atmosphere in this region, so that NO was reduced rapidly. Nevertheless, when $R_{2\text{-}12}$ was too high, the slow mixing of reactants under this interaction was detrimental to the early formation of the reductive region, so that the generated NO couldn't be reduced timely. Additionally, in this region, the change of NO concentration was different significantly when $R_{2\text{-}12}$= 1.00 or 3.00 under different λ_2, indicating that λ_2 influenced the effect of the interaction on the NO concentration distribution. Below 1400 mm, NO concentration under $R_{2\text{-}12}$<1.00 was lower than that under $R_{2\text{-}12}$>1.00, which was mainly related to the denitration capacity of the upper reduction region. When $R_{2\text{-}12}$ was lower, the better denitration capacity could promote the early removal and reduction of coal-N, and thus reduce the possibility of the subsequent NO generation.

3.2.2.3 Combustion efficiency and NO_x emission

Fig. 11 shows the effect of the interaction regulated by varying $R_{2\text{-}12}$ on combustion efficiency and NO_x emission. When λ_2=0.40, NO_x emission increased, while it decreased slightly first and then increased, and reached the minimum under $R_{2\text{-}12}$ = 0.33 when λ_2=0.50 and 0.60, which indicated that the total secondary air flow influenced the effect of this interaction on the NO_x

emission greatly. For the former, the axial secondary air dominated gradually as $R_{2\text{-}12}$ increased, so that the mixing of reactants was slow and the formation of the reduction region was delayed, which limited the advantages of the air-staged technology. Moreover, though the axial secondary air flow increased gradually as $R_{2\text{-}12}$ increased, the increase wasn't obvious due to the lower λ_2, which couldn't promote the release of coal-N effectively in the upper part of DFC. Hence, the above synergy resulted in the decrease of denitrification efficiency in the reduction region. For the latter, the axial secondary air flow was higher than that for the former under certain $R_{2\text{-}12}$. Though the denitrification intensity in the reduction region was limited as $R_{2\text{-}12}$ increased, the action was smaller when $R_{2\text{-}12}$ only increased from 0.00 to 0.33, and conversely the introduction of more combustion air from the top of the DFC might promote the cleavage of carbon chains and the early release of coal-N. Moreover, the higher radial secondary air intensified the mixing of reactants, which accelerated the formation of the reduction region. Hence, when λ_2 was higher, the positive effect on the NO_x emission was stronger than the adverse effect with the slight increase of $R_{2\text{-}12}$, and it also indicated that it was beneficial for the early release of coal-N and NO_x reduction emission to introduce the axial secondary air properly. Nevertheless, as $R_{2\text{-}12}$ continued to increase, the adverse effect reinforced gradually, and begun to dominate instead of the positive effect, so that the coal-N in the reduction region couldn't be removed well and the possibility of the subsequent NO_x generation increased.

Under different λ_2, the change trend of the combustion efficiency was different as $R_{2\text{-}12}$ increased, indicating that the total secondary air flow influenced the effect of the interaction on the combustion efficiency. When $\lambda_2 = 0.40$, the combustion efficiency increased first and then decreased as $R_{2\text{-}12}$ increased. Increasing $R_{2\text{-}12}$ properly could prolong the combustion time due to the introduction of the more axial secondary air. Nevertheless, when $R_{2\text{-}12}$ increased to a high level, the mixing and combustion of reactants was slow under this interaction due to the higher proportion of the axial secondary air flow, so that the combustion was deteriorated gradually as $R_{2\text{-}12}$ increased. When $\lambda_2 = 0.50$, the combustion efficiency almost remained constant as $R_{2\text{-}12}$ increased. The reason might be that the combustion efficiency had reached a high level in this condition, so that it was difficult to optimize the combustion further only by adjusting the secondary air distribution, which also indicated that the interaction had less effect on the combustion efficiency under this λ_2. When λ_2=0.60, the combustion efficiency remained a high level first and then decreased to a low level as $R_{2\text{-}12}$ increased. When $R_{2\text{-}12}$ was lower, the adverse effect of the axial secondary air on the combustion wasn't obvious due to the lower proportion of it flow. Moreover, under this λ_2, the higher total secondary air flow could prolong the combustion time and promote the burnout, which ensured a high burnout level, so that the change of the interaction was difficult to improve the combustion further in this condition as $R_{2\text{-}12}$ increased. Nevertheless, when $R_{2\text{-}12}$ was higher, the mixing and combustion of reactants were deteriorated greatly under the adverse effect of the axial secondary air.

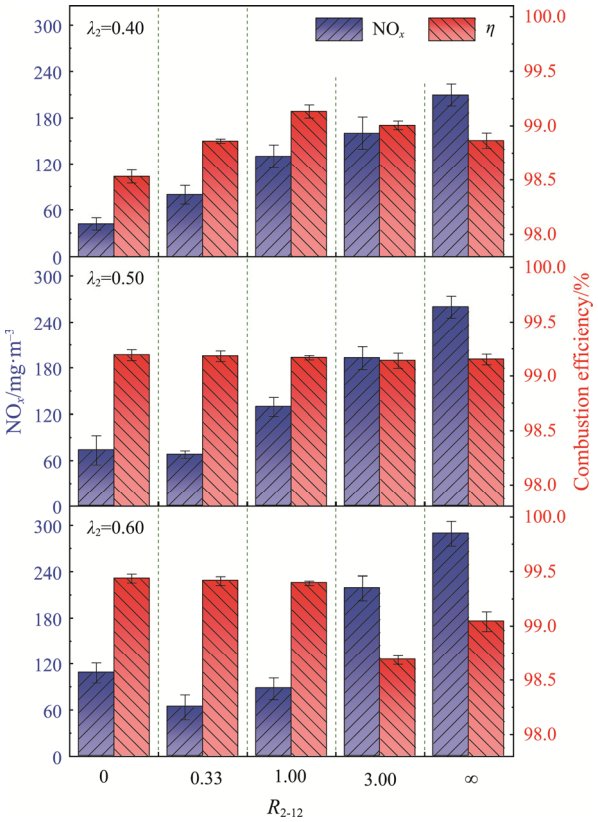

Fig. 11 Combustion efficiency and NO_x emission

In conclusion, the interaction regulated by varying $R_{2\text{-}12}$ influenced the combustion efficiency and NO_x emission greatly, and this effect was regulated by λ_2. When λ_2 was lower, the NO_x emission decreased as $R_{2\text{-}12}$ decreased, while the combustion efficiency might also decreased, meaning the low emission and high efficiency weren't realized in the meantime. When λ_2 was higher, the lower $R_{2\text{-}12}$ was more conducive to realize the clean and efficient combustion.

3.3 The effect of reductive intensity in the reduction region on combustion characteristics and NO_x emission

Among the above 15 cases, NO_x emission in Case 1 (λ_2=0.40, $R_{2\text{-}12}$=0) reached the minimum, and it was only

41.75 mg/m^3 (@6%O_2), achieving the ultra-low NO_x emission during combustion. Nevertheless, the combustion efficiency was also the lowest at 98.53%. Liu [50] found the early introduction of the partial tertiary air could improve the combustion effectively in the DFC, while reduce the reductive intensity correspondingly in the reduction region, meaning that the change of the reductive intensity regulated by varying $R_{3\text{-}12}$ affected the subsequent combustion and emission obviously. Hence, to explore the methods in depth to achieve the clean and efficient combustion, the effect of the reductive intensity in the reduction region on the combustion characteristics and NO_x emission was investigated by varying $R_{3\text{-}12}$ based on case 1.

3.3.1 Temperature distribution

Fig. 12 shows the effect of the reductive intensity regulated by varying $R_{3\text{-}12}$ on the temperature distribution along the DFC. Under different $R_{3\text{-}12}$, all the temperature curves had basically the same trend: increase first and then decrease. With the introduction of the first-staged tertiary air (except $R_{3\text{-}12}$=0.00), the position of the peak temperature point was shifted down from 600 mm to 1200 mm, which was mainly due to the significant increase in the combustion intensity of the residual fuel in the vicinity of 1000 mm. Moreover, as $R_{3\text{-}12}$ increased, the combustion intensity in the main combustion region increased continuously, so that the peak temperature at 1200 mm increased gradually.

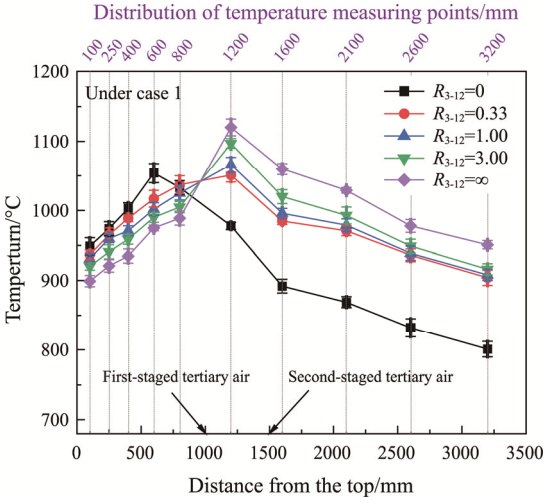

Fig. 12 The temperature distribution of DFC

3.3.2 Flus gas analysis

Fig. 13 shows the effect of the reductive intensity regulated by varying $R_{3\text{-}12}$ on O_2, CO_2 and CO concentrations along the DFC. Above 900 mm, O_2 concentration curves under different $R_{3\text{-}12}$ almost overlapped, indicating that $R_{3\text{-}12}$ had less effect on the O_2 concentration distribution in this region. At 1400 mm, with the introduction of the first-staged tertiary air, O_2 in the flue gas was replenished, so that O_2 concentration increased significantly. Nevertheless, though the amount of O_2 supplied from the first-staged tertiary air increased gradually as $R_{3\text{-}12}$ increased, correspondingly O_2 consumption was also accelerated due to the increase in the mixing intensity of reactants, so that O_2 concentration at 1400 mm didn't show a certain pattern with increasing $R_{3\text{-}12}$ under this synergy. Below 2400 mm, the difference of O_2 concentration under different $R_{3\text{-}12}$ was mainly caused by the different combustion effect of the residual fuel in the middle of the DFC.

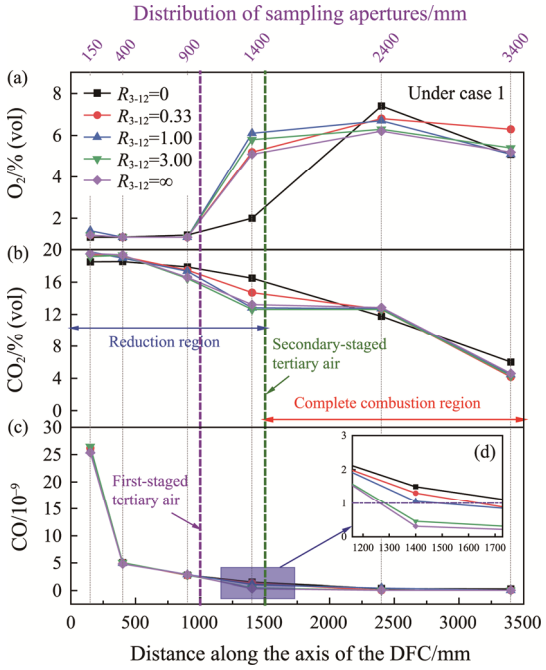

Fig. 13 O_2, CO_2 and CO concentrations along the DFC

Above 900 mm, there was a small difference in the CO_2 concentration distribution under different $R_{3\text{-}12}$. Afterwards, with the introduction of the first-staged tertiary air, CO_2 concentration decreased significantly at 1400 mm due to the dilution of the flue gas, and the increase of O_2 concentration in this position also confirmed this analysis. In the lower part of the DFC, since a large amount of organic carbon in the preheated fuel had been released, the combustible carbon entered into this region was less, so that the CO_2 concentration distribution had a small difference under different $R_{3\text{-}12}$.

In terms of the distribution of O_2 and CO_2 concentrations under different $R_{3\text{-}12}$, it could be inferred that the reductive intensity regulated by varying $R_{3\text{-}12}$ mainly influenced the combustion in the middle of the DFC.

All the CO concentration curves had the same trend: decreasing to a low level rapidly first, and then remaining

constant. At 1400 mm, CO concentration decreased gradually as $R_{3\text{-}12}$ increased, which was mainly due to the rapid homogeneous consumption of the coal gas by the first-staged tertiary air, and this consumption was promoted constantly as $R_{3\text{-}12}$ increased, so that CO content in the flue gas decreased gradually.

Fig. 14 shows the effect of the reductive intensity regulated by varying $R_{3\text{-}12}$ on NO and NO_2 concentrations along the DFC. Above 900 mm, the change of NO concentration under different $R_{3\text{-}12}$ was unconspicuous, indicating that $R_{3\text{-}12}$ had less effect on the NO concentration distribution in this region. Afterwards, with the introduction of the first-staged tertiary air, NO concentration begun to increase at 1400 mm, and it was always higher than that under case 1 below 1400 mm, which was mainly due to the decrease in the reductive intensity in the region of 1000–1500 mm. Hence, the reductive intensity regulated by varying $R_{3\text{-}12}$ influenced the NO concentration distribution greatly in the lower part of the DFC.

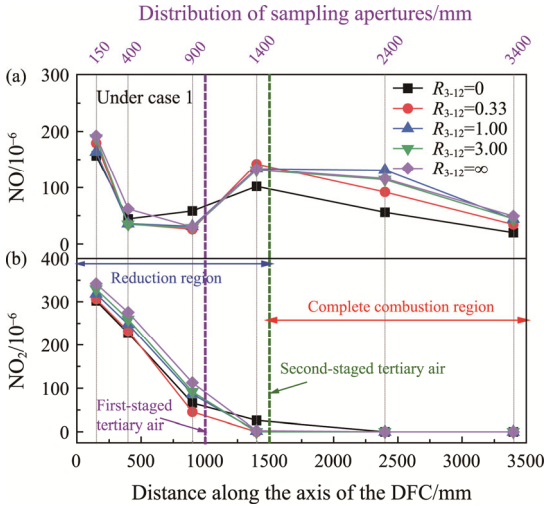

Fig. 14 NO and NO_2 concentrations along the DFC

With the introduction of the first-staged tertiary air, the consumption and decomposition of NO_2 were accelerated greatly in the vicinity of 1000 mm, so that NO_2 concentration decreased slightly at 1400 mm. Afterwards, since unstable NO_2 had been almost depleted above 1400 mm, there were small differences in the NO_2 concentration distribution under different $R_{3\text{-}12}$ in the lower part of the DFC.

3.3.3 Combustion efficiency and NO_x emission

Fig. 15 shows the effect of the reductive intensity regulated by varying $R_{3\text{-}12}$ on NO_x emission and combustion efficiency. As $R_{3\text{-}12}$ increased from 0.00 to 1.00, NO_x emission increased rapidly from 41.75 mg/m^3 to 94.36 mg/m^3, while it almost remained constant as $R_{3\text{-}12}$ continued to increase, which was mainly due to the influence of different reduction mechanisms in the region of 1000–1500 mm. As shown in Fig. 13(d), CO concentration was higher in this region when $R_{3\text{-}12}\leq 1$, more than 10^{-3}, indicating the coal gas played an important role in the NO_x reduction. Hence, as $R_{3\text{-}12}$ increased, the homogeneous reduction efficiency decreased gradually due to the decrease in the CO concentration, so that NO_x emission increased. Nevertheless, when $R_{3\text{-}12}>1$, CO concentration was extremely low in the region, meaning that NO_x was mainly reduced by the coal char rather than the coal gas. Hence, as $R_{3\text{-}12}$ increased, the mixing of the coal char and flue gas was reinforced and the NO_x heterogeneous reduction efficiency increased in this region. Moreover, the intense mixing also promoted the release of coal-N, so that NO_x emission almost remained constant under the synergy of the above effects. The results revealed that the reductive intensity regulated by varying $R_{3\text{-}12}$ had different influences on the NO_x emission under homogeneous to heterogeneous reduction mechanisms. Additionally, it could be found that the NO_x emission was almost the same when $R_{3\text{-}12}$=1.00 and 3.00. For the former, the NO_x reduction efficiency was higher due to the higher CO concentration, but the release rate of coal-N was lower compared to the latter, leading the total coal-N reduction amount was limited greatly. Hence, under the synergy of the reduction intensity and the coal-N release rate, both of the NO_x emission were still the same.

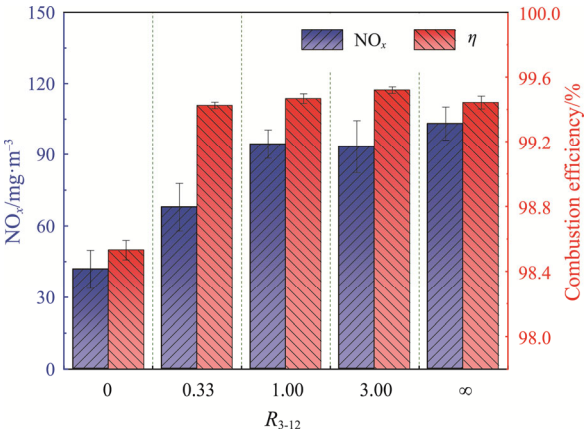

Fig. 15 Combustion efficiency and NO_x emission

The combustion efficiency increased rapidly from 98.53% to 99.42% as $R_{3\text{-}12}$ increased from 0.00 to 0.33, indicating that increasing $R_{3\text{-}12}$ properly could improve the combustion effectively. Nevertheless, as $R_{3\text{-}12}$ continued to increase, the combustion efficiency was hardly changed. Since the combustion efficiency had been high enough when $R_{3\text{-}12}$=0.33, indicating the content of combustible compositions in the residual fuel was extremely low, it was difficult to improve the combustion

further only by adjusting the tertiary air distribution. The results revealed that reducing the reductive intensity properly could optimize the combustion effectively, while with its excessive decrease, the combustion couldn't be optimized further.

In summary, the reductive intensity regulated by varying $R_{3\text{-}12}$ affected the NO_x emission and combustion efficiency significantly. As the reductive intensity decreased properly, the combustion efficiency increased obviously, while the NO_x emission increased due to the decrease in the homogeneous reduction efficiency under the homogeneous reduction mechanism. Nevertheless, as the reductive intensity decreased excessively, the combustion efficiency hardly increased further, and the NO_x emission was also unchanged under the heterogeneous reduction mechanism. Hence, in terms of the practical industrial demands, adjusting the reductive intensity properly to achieve a perfect balance between the de-NO_x emission and high combustion efficiency during combustion was very necessary.

4. Conclusion

The effects of the interaction between the axial and radial secondary air and reductive intensity in the reduction region on the combustion and NO_x emission were investigated on a 30 kW preheating combustion test rig. The main conclusions were as follows:

(1) The self-preheating burner could maintain the stable operation without the external heat imput for a long time when λ_P=0.35, and the operating temperature was within 900°C. NO_x and O_2 in the preheating coal gas were not detected, and the released coal-N during preheating was converted into N_2, HCN and NH_3.

(2) The interaction between the axial and radial secondary air and the reductive intensity in the reduction region influenced the temperature distribution significantly. As $R_{2\text{-}12}$ decreased or λ_2 increased, the interaction could cause the position of the main combustion region to shift down, and there was the interplay between the effects of $R_{2\text{-}12}$ and λ_2. As $R_{3\text{-}12}$ increased, the decrease in the reductive intensity could also cause the position of the main combustion region to shift down, and the peak temperature increased gradually in this region.

(3) The interaction between the axial and radial secondary air and the reductive intensity in the reduction region influenced the release of fuel-N along the DFC and NO_x emission significantly. As λ_2 or $R_{2\text{-}12}$ increased, the interaction influenced the NO_x reduction adversely in the DFC, and there was a mutual promotion between these two influences. Moreover, when λ_2 or $R_{2\text{-}12}$ was higher, the adverse effect of the interaction on the NO_x reduction was extended all the way to the lower part of the DFC, so that the NO_x emission increased obviously as λ_2 or $R_{2\text{-}12}$ increased in this condition. When $R_{2\text{-}12}$ was lower, the interaction could promote the release of fuel-N at the top of the DFC and accelerate the formation of the reduction region. As $R_{3\text{-}12}$ increased, the decrease in the reduction intensity influenced the NO_x emission differently under the homogeneous to heterogeneous reduction mechanisms. Under the homogeneous reduction mechanism, the NO_x emission increased gradually as the decrease in the reduction intensity, while it almost remained constant at a high level under the heterogeneous reduction mechanism.

(4) The interaction between the axial and radial secondary air and the reductive intensity in the reduction region influenced the combustion efficiency obviously. λ_2 and $R_{2\text{-}12}$ influenced the effect of the interaction on the combustion efficiency jointly. When $R_{2\text{-}12}$ was lower, the interaction could improve the combustion efficiency as λ_2 increased, while when $R_{2\text{-}12}$ was higher, it influenced the combustion adversely as λ_2 increased excessively, so that the combustion efficiency decreased. As $R_{3\text{-}12}$ increased properly, the decrease in the reductive intensity could cause the combustion efficiency to increase obviously, while the combustion efficiency was hardly improved further with the continuous decrease in the reductive intensity when $R_{3\text{-}12}$ increased excessively.

(5) The combustion efficiency was above 98% in all the cases. When $R_{2\text{-}12}$=0.00, λ_2=0.40 and $R_{3\text{-}12}$=0.00, the NO_x emission was only 41.75 mg/m^3 under this interaction and reductive intensity, indicating that the NO_x emission could reach the ultra-low level without sacrificing the combustion efficiency. Based on the above conditions, optimizing the interaction and reduction intensity could improve the combustion efficiency obviously by increasing λ_2, $R_{2\text{-}12}$ and $R_{3\text{-}13}$ properly, while correspondingly the NO_x emission also increased slightly. Hence, to realize the high combustion efficiency and ultra-low NO_x emission simultaneously, the increase range of λ_2, $R_{2\text{-}12}$ and $R_{3\text{-}13}$ should be controlled strictly.

Acknowledgment

Youth Innovation Promotion Association, CAS (2019148), CAS Project for Young Scientists in Basic Research (YSBR-028), and the National Natural Science Foundation of China (No. 52006233) are gratefully acknowledged.

Conflict of Interest

On behalf of all authors, the corresponding author states that there is no conflict of interest.

References

[1] Chai J., Du M., Liang T., Sun X., Yu J., Zhang Z., Coal consumption in China: how to bend down the curve. Energy Economics, 2019, 80: 38–47.

[2] Zou C., Zhao Q., Zhang G., Xiong B., Energy revolution: From a fossil energy era to a new energy era. Natural Gas Industry B, 2016, 3: 1–11.

[3] De F., Lu Z., Streets D., Satellite NO_2 retrievals suggest China has exceeded its NO_x reduction goals from the twelfth Five-Year Plan. Scientific reports, 2016, 6: 35912.

[4] Gong Z., Zhang H., Juan Y., Zhu L., Zheng W., Ding J., A review of application and development of combustion technology for oil sludge. Journal of Environmental Science and Health, Part A-Toxic, 2022, 57: 396–412.

[5] Kuang M., Li Z., Zhang Y., Chen X., Jia J., Zhu Q., Asymmetric combustion characteristics and NO_x emissions of a down-fired 300 MW_e utility boiler at different boiler loads. Energy, 2012, 37: 580–590.

[6] Kuang M., Li Z., Ling Z., Zeng X., Evaluation of staged air and overfire air in regulating air-staging conditions within a large-scale down-fired furnace. Apply Thermal Engineering, 2014, 67: 97–105.

[7] Liu C., Hui S., Zhang X., Wang D., Zhu H., Wang X., Influence of type of burner on NO emissions for pulverized coal preheating method. Apply Thermal Engineering, 2015, 85: 278–286.

[8] Fan W., Lin Z., Kuang J., Li Y., Impact of air staging along furnace height on NO_x emissions from pulverized coal combustion. Fuel Processing Technology, 2010, 91: 625–634.

[9] Sung Y., Moon C., Eom S., Choi G., Kim D., Coal-particle size effects on NO reduction and burnout characteristics with air-staged combustion in a pulverized coal-fired furnace. Fuel, 2016, 182: 558–567.

[10] Zhou Q., Zhao Q., Zhou G., Wang H., Xu T., Hui S., Comparison of combustion characteristics of petroleum coke and coal in one-dimensional furnace. Frontiers of Energy and Power Engineering in China, 2010, 4: 436–442.

[11] Zhu S., Lyu Q., Zhu J., Li J., NO emissions under pulverized char MILD combustion in O_2/CO_2 preheated by a circulating fluidized bed: Effect of oxygen-staging gas distribution. Fuel Processing Technology, 2018, 182: 104–112.

[12] Chae J., Chun Y., Effect of two-stage combustion on NO_x emissions in pulverized coal combustion. Fuel, 1991, 70: 703–707.

[13] Chen L., Zhao Y., Sun R., Sun S., Qiu P., Char structural evolution characteristics and its correlation with reactivity during NO heterogeneous NO reduction in a micro fluidized bed reaction analyzer: The influence of reaction residence time. Fuel, 2021, 296: 120648.

[14] Stadler H., Ristic D., Forster M., Schuster A., Kneer R., Scheffknecht G., NO_x-emissions from flameless coal combustion in air, Ar/O_2 and CO_2/O_2. Proceedings of the Combustion Institute, 2009, 32: 3131–3138.

[15] Abdelaal M., El-Riedy M., El-Nahas A., El-Wahsh F., Characteristics and flame appearance of oxy-fuel combustion using flue gas recirculation. Fuel, 2021, 297: 120775.

[16] Zhang S., Zhao Y., Yang J., Zhang Y., Sun P., Yu X., Simultaneous NO and mercury removal over MnO_x/TiO_2 catalyst in different atmospheres. Fuel Processing Technology, 2017, 166: 282–290.

[17] Yang W., Zhou J., Zhou Z., Lu Z., Wang Z., Liu J., Characteristics of sodium compounds on NO reduction at high temperature in NO_x control technologies. Fuel Processing Technology, 2008, 89: 1317–1323.

[18] Xu M., Wu Y., Zhang P., Liu Z., Hu Z., Lu Q., Green and moderate activation of coal fly ash and its application in selective catalytic reduction of NO with NH_3. Environmental Science & Technology, 2022, 56: 2582–2592.

[19] Cai J., Wu H., Ren Q., Lin L., Zhou T., Lyu Q., Innovative NO_x reduction from cement kiln and pilot-scale experimental verification. Fuel Processing Technology, 2020, 199: 106306.

[20] Flamme M., Low NO_x combustion technologies for high temperature applications. Energy Conversion & Management, 2001, 42: 1919–1935.

[21] Weidmann M., Verbaere V., Boutin G., Honore D., Grathwohl S., Goddard G., Detailed investigation of flameless oxidation of pulverized coal at pilot-scale (230 kW_{th}). Apply Thermal Engineering, 2015, 74: 96–101.

[22] Yan Y., Sun R., Sun L., Zhu W., Chen D., Effects of primary air velocity on co-combustion characteristics of bituminous coal and semicoke under reducing to oxidizing environment. Fuel Processing Technology, 2022, 233(2022): 107293.

[23] Shen J., Liu J., Zhang H., Jiang X., NO_x emission characteristics of superfine pulverized anthracite coal in air-staged combustion. Energy Conversion & Management, 2013, 74: 454–461.

[24] Liu W., Ouyang Z., Cao X., Na Y., Liu D., Zhu S., Effects of secondary air velocity on NO emission with coal preheating technology. Fuel, 2019, 256: 115898.

[25] Ouyang Z., Ding H., Liu W., Li S., Cao X., Effect of the staged secondary air on NO_x emission of pulverized semi-coke flameless combustion with coal preheating technology. Fuel, 2021, 291: 120137.

[26] Ding H., Ouyang Z., Zhang X., Zhu S., The effects of particle size on flameless combustion characteristics and NO_x emissions of semi-coke with coal preheating

technology. Fuel, 2021, 297: 120758.

[27] Zhu S., Lyu Q., Zhu J., Liang C., Experimental study on NO_x emissions of pulverized bituminous coal combustion preheated by a circulating fluidized bed. Journal of the Energy Institute, 2018, 92: 247–256.

[28] Zhu S., Lyu Q., Zhu J., Wu H., Wu G., Effect of air distribution on NO_x emissions of pulverized coal and char combustion preheated by a circulating fluidized bed. Energy & Fuels, 2018, 32: 7909–7915.

[29] Zhang Y., Zhu J., Lyu Q., Liu J., Pan F., Zhang J., The ultra-low NO_x emission characteristics of pulverized coal combustion after high temperature preheating. Fuel, 2020, 277: 118050.

[30] Hayhurst A., Vince I., Nitric oxide formation from N_2 in flames: The importance of "prompt" NO. Progress in Energy & Combustion Science, 1980, 6: 35–51.

[31] Ouyang Z., Song W., Li S., Liu J., Ding H., Experiment study on NO_x emission characteristics of the ultra-low volatile fuel in a 2 MW novel pulverized fuel self-sustained preheating combustor. Energy, 2020, 209: 118448.

[32] Su K., Ding H., Ouyang Z., Zhang J., Zhu S., Experimental study on effects of multistage reactant and air jet velocities on self-preheating characteristics and NO_x emission of burning pulverized coal. Fuel, 2022, 325: 124879.

[33] Thong C., Dally B., Birzer C., Kalt P., Hassan E., An experimental study on the near flow field of a round jet affected by upstream multi-lateral side-jet. Experimental Thermal & Fluid Science, 2017, 82: 198–211.

[34] Li L., Tong S., Duan L., Zhao C., Shi Z., Effect of CO_2 and H_2O on lignite char structure and reactivity in a fluidized bed reactor. Fuel Processing Technology, 2021, 211: 106564.

[35] Liu J., Liu Y., Zhu J., Ouyang Z., Man C., Zhu S., Bituminous coal deep regulated ultra-low NO_x flameless combustion with fluidized self-preheating fuel: A 2 MW_{th} experimental study. Fuel, 2021, 294: 120549.

[36] Lawal M., Fairweather M., Gogolek P., Ingham D., Ma L., Pourkashanian M., CFD predictions of wake-stabilised jet flames in a cross-flow. Energy, 2013, 53: 259–269.

[37] Mei Z., Li P., Wang F., Zhang J., Mi J., Influences of reactant injection velocities on moderate or intense low-oxygen dilution coal combustion. Energy & Fuels, 2013, 28: 369–384.

[38] Liu J., Shi J., Fu Z., Zhang J., Li Y., Ji H., Optimization study on combustion in a 1000-MW ultra-supercritical double-tangential-circle boiler. Advances in Mechanical Engineering, 2017, 9: 1–12.

[39] Jia M., Wang D., Yan C., Song J., Han Q., Chen F., Analysis of the pressure fluctuation in the flow field of a large-scale cyclone separator. Powder Technology, 2019, 343: 49–57.

[40] Jouni P., Martti J., Conversion of fuel nitrogen through HCN and NH_3 to nitrogen oxides at elevated pressure. Fuel, 1996, 75: 1377–1386.

[41] Liu W., Ouyang Z., Na Y., Cao X., Zhu S., Experimental research on NO emission with coal preheating combustion technology. Asia‐Pacific Journal of Chemical Engineering, 2020, 15: e2444.

[42] Yao Y., Zhu J., Lyu Q., Zhou Z., Experimental study on preheated combustion of pulverized semi-coke. Journal of Thermal Science, 2015, 24: 370–377.

[43] Popovic B., Thomson M., Lightstone M., The combustion efficiency of furnace exhaust gas combustors: a study of jet mixing in a reacting cross-flow. Combustion Science & Technology, 2007, 155(2007): 31–49.

[44] Lv Z., Xiong X., Yu S., Tan H., Xiang B., Huang J., Experimental investigation on NO emission of semi-coke under high temperature preheating combustion technology. Fuel, 2021, 283: 119293.

[45] Rong H., Suda T., Takafuji M., Hirata T., Sato J., Analysis of low NO emission in high temperature air combustion for pulverized coal. Fuel, 2004, 83: 1133–1141.

[46] Courtemanche B., Levendis Y., A laboratory study on the NO, NO_2, SO_2, CO and CO_2 emissions from the combustion of pulverized coal, municipal waste plastics and tires. Fuel, 1998, 77: 183–196.

[47] Lyu Q., Zhu J., Niu T., Song G., Na Y., Pulverized coal combustion and NO_x emissions in high temperature air from circulating fluidized bed. Fuel Processing Technology, 2008, 89: 1186–1192.

[48] Ouyang Z., Ding H., Liu W., Cao X., Zhu S., Effect of the primary air ratio on combustion of the fuel preheated in a self-preheating burner. Combustion Science & Technology, 2020, 194: 1247–1264.

[49] Kilpinen P., Hupa M., Homogeneous N_2O chemistry at fluidized bed combustion conditions: A kinetic modeling study. Combustion & Flame, 1991, 85: 94–104.

[50] Liu W., Ouyang Z., Na Y., Cao X., Liu D., Zhu S., Effects of the tertiary air injection port on semi-coke flameless combustion with coal self-preheating technology. Fuel, 2020, 271: 117640.